Flow difference effect in the two-lane lattice hydrodynamic model*

Wang Tao(王 涛)[a)b)], Gao Zi-You(高自友)[b)†], Zhao Xiao-Mei(赵小梅)[b)], Tian Jun-Fang(田钧方)[b)], and Zhang Wen-Yi(张文义)[b)]

[a)] *College of Automation and Electronic Engineering, Qingdao University of Science and Technology, Qingdao* 266042, *China*

[b)] *MOE Key Laboratory for Urban Transportation Complex Systems Theory and Technology, Beijing Jiaotong University, Beijing* 100044, *China*

(Received 7 December 2011; revised manuscript received 6 January 2012)

By introducing a flow difference effect, a modified lattice two-lane traffic flow model is proposed, which is proved to be capable of improving the stability of traffic flow. Both the linear stability condition and the kink–antikink solution derived from the modified Korteweg–de Vries (mKdV) equation are analyzed. Numerical simulations verify the theoretical analysis. Furthermore, the evolution laws under different disturbances in the metastable region are studied.

Keywords: traffic flow, flow difference, lattice hydrodynamic model, modified Korteweg–de VriesKdV equation

PACS: 05.70.Fh, 05.70.Jk, 64.60.F– **DOI:** 10.1088/1674-1056/21/7/070507

1. Introduction

Traffic congestion has become a serious problem in modern society. For this reason, associative issues have attracted much attention for several decades. In order to explore the underlying mechanisms of jam formation, various traffic models[1−9] such as the cellular automata model,the car-following model, the gas kinetic model (mesoscopic), and the hydrodynamic model, have been proposed. The jamming transitions between the free flow and jam flow have been observed in these models. Recently, nonlinear analysis has been widely employed to investigate traffic jams. Kurtze and Hong[10] derived the Korteweg–de Vries (KdV) equation from the macroscopic hydrodynamic model, and the traffic jam can be identified with a soliton solution of the KdV equation. Komatsu and Sasa[11] obtained the modified Korteweg–de Vries (mKdV) equation which describes traffic flow as a kink density wave with the car-following model. Taking into account the effect of acceleration delay, Nagatani and Nakanishi[12] presented an extended model and the corresponding KdV equation.

In 1998, Nagatani[13] proposed a hydrodynamical model with lattice version and derived the mKdV equation near the critical point. Subsequently, the model was widely referred to and extended, that is, revised single-lane cases, pedestrian, and so on.[14−22]

However, single-lane models are not completely consistent with reality due to the fact that a substantial proportion of the road network in most places of the world is made up of two-lane highways.[23] Therefore, two-lane traffic models will be more reasonable. In 1999, Nagatani[24] extended the single-lane model to the two-lane one. The stability of traffic flow affected by the lane change was investigated in detail. Considering the lateral effects, Tang *et al.*[25] analyzed the stability of a two-lane car-following model. Huang *et al.*[26] studied the dynamic behaviors of a continuum traffic model for a two-lane highway. Various traffic phenomena (e.g., small disturbance instability, stop-and-go waves, local clusters, and phase transition) were investigated with these models.

Under an advanced traveler information system (ATIS) environment, vehicle information, such as velocity, position, and flow, for the drivers themselves as well as the others, is available. Nevertheless, the existing studies only factor either the velocity or the position into models. Flow information may be very comprehensive since it contains both the position (density) and velocity information indirectly, and so little analytical work for the two-lane traffic flow has been

*Project supported by the National Basic Research Program of China (Grant No. 2012CB725400), the National Natural Science Foundation of China (Grant Nos. 71131001, 71071012, and 11001143), and the Fundamental Research Funds for the Central Universities of China (Grant No. 2011YJS235).

†Corresponding author. E-mail: zygao@bjtu.edu.cn

© 2012 Chinese Physical Society and IOP Publishing Ltd

implemented up to now.

In this paper, we present a new lattice model considering the flow difference effect (FDE) for a two-lane highway. The linear stability and nonlinear analysis method are employed to investigate some characteristics of the new model. In addition, the evolution laws under different disturbances in the metastable region in low- and high-density conditions are also performed.

This paper is organized as follows. The original model and the new model are given in Section 2. Section 3 provides a linear stability analysis. Applying the reductive perturbation method, we obtain the mKdV equation around the critical point in Section 4. In Section 5, numerical simulations will be carried out. Finally in Section 6, a conclusion is drawn.

2. Model

2.1. Origin model

The origin two-lane lattice hydrodynamical traffic model is exhibited in Fig. 1. When the density at site $j-1$ on the lane 2 is higher than that at site j on the lane 1, the change from lane 2 to lane 1 will occur at the following rate: $\gamma|\rho_0^2V'(\rho_0)|(\rho_{2,j-1}(t)-\rho_{1,j}(t))$, where γ is a fixed dimensionless coefficient, constant $|\rho_0^2V'(\rho_0)|$ is introduced to ensure that it is dimensionless. Accordingly, if the density at site j on the lane 1 is higher than that at site $j+1$ on the lane 2, the change from lane 1 to lane 2 will occur at the following rate $\gamma|\rho_0^2V'(\rho_0)|(\rho_{1,j}(t)-\rho_{2,j+1}(t))$.

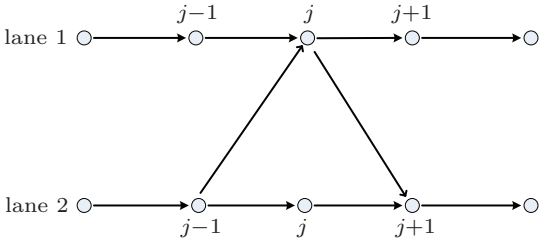


Fig. 1. Schematic model of traffic flow on a two-lane highway.

The two-lane lattice hydrodynamic traffic model is formulated as follows.[24] The continuity equation for lane 1 is

$$\begin{aligned}&\partial_t\rho_{1,j}(t)+\rho_0(\rho_{1,j}(t)v_{1,j}(t)-\rho_{1,j-1}(t)v_{1,j-1}(t))\\&=\gamma|\rho_0^2V'(\rho_0)|(\rho_{2,j+1}(t)-2\rho_{1,j}(t)+\rho_{2,j-1}(t)).\end{aligned}\quad(1)$$

The continuity equation for lane 2 is

$$\begin{aligned}&\partial_t\rho_{2,j}(t)+\rho_0(\rho_{2,j}(t)v_{2,j}(t)-\rho_{2,j-1}(t)v_{2,j-1}(t))\\&=\gamma|\rho_0^2V'(\rho_0)|(\rho_{1,j+1}(t)-2\rho_{2,j}(t)+\rho_{1,j-1}(t)),\end{aligned}\quad(2)$$

where ρ_0 is the average density, and ρ and v denote the local density and the local velocity, respectively. Symbol t indicates the time index. As for the binary subscript (i,j) $(i,j=1,2)$, the former expresses the lane label and the latter represents the site on the two-lane highway. The $V(\cdot)$ is the optimal velocity function that decreases monotonically, bounds upper and inflects the point at $\rho=\rho_{\rm c}$ when $\rho_0=\rho_{\rm c}$. For simplicity, t will be neglected hereafter.

Accordingly, Nagatani[24] developed a lattice version of the continuum model for the two-lane highway is described by continuity Eq. (3) obtained by adding Eq. (1) to Eq. (2) and the following equation:

$$\begin{aligned}&\partial_t\rho_j+\rho_0(\rho_jv_j-\rho_{j-1}v_{j-1})\\&=\gamma|\rho_0^2V'(\rho_0)|(\rho_{j+1}-2\rho_j+\rho_{j-1}),\end{aligned}\quad(3)$$

$$\partial_t(\rho_jv_j)=a\rho_0V_e(\rho_{j+1})-a\rho_jv_j,\quad(4)$$

where

$$\begin{aligned}\rho_j&=(\rho_{1,j}+\rho_{2,j})/2,\\\rho_jv_j&=(\rho_{1,j}v_{1,j}+\rho_{2,j}v_{2,j})/2,\\V_{\rm e}(\rho_j)&=(V(\rho_{1,j})+V(\rho_{2,j}))/2.\end{aligned}$$

2.2. The modified model

In this section, we will introduce a new lattice hydrodynamic model for the two-lane highway. Compared with Nagatani's model,[24] the modified model takes the FDE between a lattice and its predecessor into account, leading to a novel evolution equation below.

$$\begin{aligned}\partial_t(\rho_jv_j)=\;&a\rho_0V_{\rm e}(\rho_{j+1})-a\rho_jv_j\\&+\lambda(\rho_{j+1}v_{j+1}-\rho_jv_j),\end{aligned}\quad(5)$$

where λ is the react coefficient of flow difference between the leading and following lattice, the other variables mean the same as those in Eqs. (3) and (4).

Eliminating velocity v in Eqs. (3) and (5), we acquire the following density equation:

$$\begin{aligned}&\partial_t^2\rho_j+a\rho_0^2(V_{\rm e}(\rho_{j+1})-V_{\rm e}(\rho_j))\\&-ma\gamma|\rho_0^2V'(\rho_0)|(\rho_{j+1}-2\rho_j\\&+\rho_{j-1})+a\partial_t\rho_j+\lambda\gamma|\rho_0^2V'(\rho_0)|\\&\times(\rho_{j+2}-3\rho_{j+1}+3\rho_j-\rho_{j-1})\\&-\lambda(\partial_t\rho_{j+1}-\partial\rho_j)-\gamma|\rho_0^2V'(\rho_0)|\\&\times(\partial_t\rho_{j+1}-2\partial_t\rho_j+\partial_t\rho_{j-1})=0.\end{aligned}\quad(6)$$

The optimal velocity function[24] adopted here is

$$V(\rho)=\tanh\left(\frac{2}{\rho_0}-\frac{\rho}{\rho_0^2}-\frac{1}{\rho_{\rm c}}\right)+\tanh\left(\frac{1}{\rho_{\rm c}}\right).\quad(7)$$

For the convenience of analysis, we will simplify $V_{\rm e}(\rho)$ as $V(\rho)$ hereafter.

3. Linear stability analysis

We apply the linear stability analysis method to investigate the influence of relative FDE in the two-lane lattice hydrodynamic model. Assuming the initial steady state (i.e., uniform traffic flow with a constant density ρ_0 and optimal velocity $V(\rho_0)$), the steady-state solution can be written as

$$\rho_j(t) = \rho_0, \quad v_j(t) = V(\rho_0). \tag{8}$$

Let $y_j(t)$ be a small deviation from the steady-state density: $\rho_j(t) = \rho_0 + y_j(t)$, and $y_j(t) = \exp(\,\mathrm{i}kj + zt)$. Then, we obtain

$$\begin{aligned}
&V(\rho_j) = V(\rho_0) + V'(\rho_0)y_j(t),\\
&V(\rho_{j+1}) = V(\rho_0) + V'(\rho_0)y_{j+1}(t), &(9)\\
&y_{j-1}(t) = y_j(t)\exp(-\mathrm{i}k),\\
&y_{j+1}(t) = y_j(t)\exp(\mathrm{i}k), &(10)\\
&\partial_t\rho_{j-1} = zy_{j-1}(t), \quad \partial_t\rho_j = zy_j(t), &(11)\\
&\partial_t\rho_{j+1} = zy_{j+1}(t), \quad \partial_t^2\rho_j = z^2y_j(t), &(12)
\end{aligned}$$

where

$$V'(\rho_0) = \frac{\mathrm{d}V(\rho)}{\mathrm{d}\rho}|_{\rho=\rho_0}.$$

Substituting Eqs. (9)–(12) into Eq. (6), we have

$$\begin{aligned}
&z^2 + a\rho_0^2V'(\rho_0)(\mathrm{e}^{\mathrm{i}k} - 1)\\
&- a\gamma|\rho_0^2V'(\rho_0)|(\mathrm{e}^{\mathrm{i}k} + \mathrm{e}^{-\mathrm{i}k} - 2) + az\\
&+ \lambda\gamma|\rho_0^2V'(\rho_0)|(\mathrm{e}^{\mathrm{i}2k} - 3\mathrm{e}^{\mathrm{i}k} + 3 - \mathrm{e}^{-\mathrm{i}k}) - \lambda z(\mathrm{e}^{\mathrm{i}k} - 1)\\
&- \gamma|\rho_0^2V'(\rho_0)|z(\mathrm{e}^{\mathrm{i}k} + \mathrm{e}^{-\mathrm{i}k} - 2) = 0. \qquad (13)
\end{aligned}$$

Let $z = \mathrm{i}u$ and substituting it into Eq. (13), setting both the real part and imaginary part of Eq. (13) zero, we obtain

$$\begin{aligned}
&- u^2 + a\rho_0^2V'(\rho_0)(\cos k - 1)\\
&- 2a\gamma|\rho_0^2V'(\rho_0)|(\cos k - 1)\\
&+ \lambda\gamma|\rho_0^2V'(\rho_0)|(\cos 2k - 4\cos k + 3)\\
&+ \lambda u\sin k = 0, \qquad (14)\\
&a\rho_0^2V'(\rho_0) + au + \lambda\gamma|\rho_0^2V'(\rho_0)|(\sin 2k - 2\sin k)\\
&- \lambda u(\cos k - 1) - 2u\gamma|\rho_0^2V'(\rho_0)|(\cos k - 1) = 0. \qquad (15)
\end{aligned}$$

It can be further derived from Eq. (15) that

$$u = -\frac{|\rho_0^2V'(\rho_0)|[2\lambda\gamma(\cos k - 1) - a]\sin k}{[2\gamma|\rho_0^2V'(\rho_0)| - \lambda](\cos k - 1) + a}. \tag{16}$$

Substituting Eq. (16) into Eq. (14) and assuming $k \to 0$, we obtain the stability condition

$$a > -\frac{2\rho_0^2V'(\rho_0)}{1 + 2\gamma} - \frac{2\lambda}{1 + 2\gamma}. \tag{17}$$

When $\lambda = 0$, equation (17) is reduced to the stability condition of Nagatani's model[23]

$$a > -\frac{2\rho_0^2V'(\rho_0)}{1 + 2\gamma}. \tag{18}$$

If $\gamma = 0$, equation (17) is reduced to the stability condition of single lane model

$$a > -2\rho_0^2V'(\rho_0) - 2\lambda. \tag{19}$$

Comparing Eq. (17) with Eqs. (18) and (19), we find that both the lane change and FDE can improve the traffic flow stability with increasing γ and λ.

4. Nonlinear stability analysis

Using the reduced perturbation method, we obtain the mKdV equation to describe the traffic jam around the critical point. First, we introduce slow scales for the space variable j and time variable t, and define the slow variables X and T for $0 < \varepsilon \ll 1$ as follows:

$$X = \varepsilon(j + bt), \quad T = \varepsilon^3t, \tag{20}$$

where b is a constant to be determined. We define the density $\rho_j(t)$ as

$$\rho_j(t) = \rho_\mathrm{c} + \varepsilon R(X, T). \tag{21}$$

By expanding Eq. (6) to the fifth order of ε with respect to the slow variables X and T, we obtain the following nonlinear equation:

$$\begin{aligned}
&\varepsilon^2[a\rho_\mathrm{c}^2V'(\rho_\mathrm{c}) + ab]\partial_XR\\
&+ \varepsilon^3\left[b^2 + \frac{a\rho_\mathrm{c}^2V'(\rho_\mathrm{c})}{2} + \gamma a\rho_\mathrm{c}^2V'(\rho_\mathrm{c}) - b\lambda\right]\partial_X^2R\\
&+ \varepsilon^4\left\{\left[\frac{a\rho_\mathrm{c}^2V'(\rho_\mathrm{c})}{6} - \lambda\gamma\rho_\mathrm{c}^2V'(\rho_\mathrm{c}) - \frac{b\lambda}{2}\right.\right.\\
&\left.\left.+ \gamma b\rho_\mathrm{c}^2V'(\rho_\mathrm{c})\right]\partial_X^3R + \frac{a\rho_\mathrm{c}^2V'''(\rho_\mathrm{c})}{6}\partial_XR^3 + a\partial_TR\right\}\\
&+ \varepsilon^5\left\{(2b - \lambda)\partial_T\partial_XR + \left[\frac{a\rho_\mathrm{c}^2V'(\rho_\mathrm{c})}{24}\right.\right.\\
&\left.\left.+ \frac{a\gamma\rho_\mathrm{c}^2V'(\rho_\mathrm{c})}{12} - \frac{\gamma\lambda\rho_\mathrm{c}^2V'(\rho_\mathrm{c})}{2} - \frac{b\lambda}{6}\right]\partial_X^4R\right.\\
&\left.+ \frac{a\rho_\mathrm{c}^2V'''(\rho_\mathrm{c})}{12}\partial_X^2R^3\right\} = 0. \qquad (22)
\end{aligned}$$

Near the critical point, we have $a_\mathrm{c} = a(1+\varepsilon^2)$. Assuming $b = -\rho_\mathrm{c}^2V'(\rho_\mathrm{c})$ and eliminating the second-order and third-order terms of Eq. (21), we obtain

$$\begin{aligned}
&\varepsilon^4[\partial_TR - g_1\partial_X^3R + g_2\partial_XR^3]\\
&+ \varepsilon^5[g_3\partial_X^2R + g_4\partial_X^4R + g_5\partial_X^2R^3] = 0, \qquad (23)
\end{aligned}$$

where

$$g_1 = -\frac{\rho_c^2 V'(\rho_c)}{6}\left[1 - \frac{6\lambda\gamma}{a_c} + \frac{3\lambda}{a_c} - \frac{6\gamma\rho_c^2 V'(\rho_c)}{a_c}\right],$$
$$g_2 = \frac{\rho_c^2 V'''(\rho_c)}{6}, \quad g_3 = \frac{-\rho_c^2 V'(\rho_c)}{2}(1+2\gamma),$$
$$g_4 = \frac{\rho_c^2 V'(\rho_c)}{6a_c}[2\rho_c^2 V'(\rho_c) + \lambda])$$
$$\times\left[1 - \frac{6\lambda\gamma}{a_c} + \frac{3\lambda}{a_c} - \frac{\gamma\rho_c^2 V'(\rho_c)}{a_c}\right]$$
$$+\frac{\rho_c^2 V'(\rho_c)}{24a_c}(a_c + 2a_c\gamma - 12\lambda\gamma + 4\lambda),$$
$$g_5 = \frac{\rho_c^2 V'''(\rho_c)}{12} + \frac{\rho_c^4 V'(\rho_c)V'''(\rho_c)}{3a_c}.$$

When $T' = g_1 T$ and $R = \sqrt{g_1/g_2}R'$, the corresponding standard mKdV equation for Eq. (23) can be deduced as

$$\partial_{T'} R' - \partial_X^3 R' + \partial_X R'^3 + \varepsilon M[R'] = 0, \qquad (24)$$

where

$$M[R'] = \frac{1}{g_1}\left(g_3\partial_X^2 R' + \frac{g_1 g_5}{g_2}\partial_X^2 R'^3 + g_4\partial_X^4 R'\right).$$

Ignoring the $O(\varepsilon)$ term in Eq. (24), we obtain the mKdV equation with the kink–antikink solution

$$R_0'(X,T') = \sqrt{c}\tanh[\sqrt{\frac{c}{2}}(X - cT')]. \qquad (25)$$

When $R'(X,T') = R_0'(X,T') + \varepsilon R_1'(X,T')$, in order to determine the selected value of the propagation velocity for the kink–antikink solution, it is necessary to satisfy the following condition:

$$(R_0', M[R_0']) \equiv \int_{-\infty}^{+\infty} \mathrm{d}X R_0' M[R_0'] = 0, \qquad (26)$$

where $M[R_0'] = M[R']$. By solving Eq. (26), we obtain[27]

$$c = \frac{5g_2 g_3}{2g_2 g_4 - 3g_1 g_5}. \qquad (27)$$

Hence, we derive the kink–antikink solution $(-\rho_c^2 V'(\rho_c) = 1,\ \rho_c^6 V'''(\rho_c) = 2)$

$$\rho_j = \rho_c + \varepsilon\sqrt{\frac{g_1 c}{g_2}}\tanh(\sqrt{\frac{c}{2}}(X - cg_1 T)), \qquad (28)$$

where $\varepsilon^2 = a_c/a - 1$. The amplitude A of the solution is

$$A = \sqrt{\frac{g_1}{g_2}\varepsilon^2 c}. \qquad (29)$$

The kink–antikink solution represents the coexisting phase, which includes both freely moving phase (within low density) and jamming phase (within high density). The density of the freely moving phase is given by $\rho = \rho_c - A$, and the density of the jamming phase is given by $\rho = \rho_c + A$. Then, the coexisting curve in the density-sensitivity space is obtained.

Figure 2 shows the coexisting curves and neutral stability curves in the density-sensitive space without lane changing ($\gamma = 0$, see Fig. 2(a)) and with lane changing ($\gamma = 0.1$, see Fig. 2(b)). The apex of each curve indicates the critical point. For each pair of curves, the space is divided into three regions, i.e., the stable region, the metastable region, and the unstable region. We can observe that the stable region in Fig. 2(b) is obviously larger than the corresponding region in Fig. 2(a), which means that the lane change can enhance the traffic flow stability. Moreover, Figure 2 shows that in view of FDE, the critical points, the coexisting curves, and the neutral stability curves become lower, which means that the stability of the uniform traffic flow has been further enhanced.

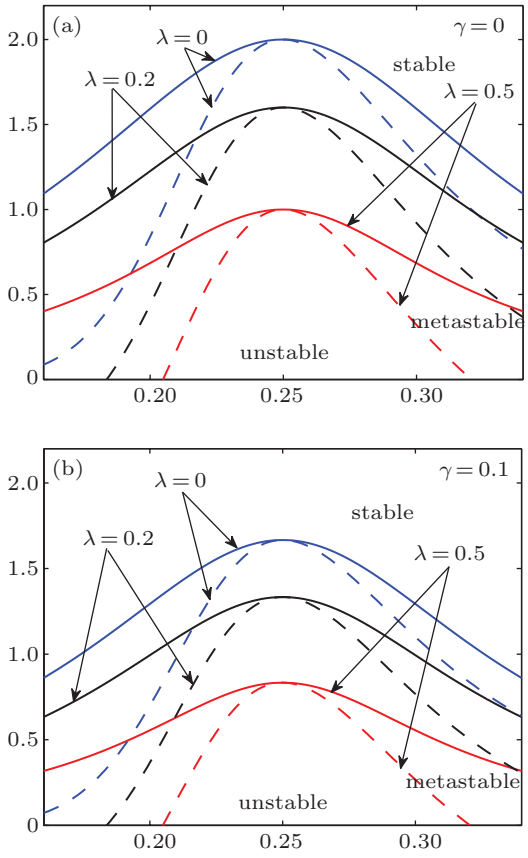


Fig. 2. (colour online) Phase diagram of (ρ, a) plane (a) without lane change, and (b) with lane change. The solid curves and dotted lines denote the coexisting curves and neutral stability lines, respectively, for $\lambda = 0.0,\ 0.2$, and 0.5.

5. Numerical simulation

For convenience, we rewrite Eq. (6) in the difference form

$$\begin{aligned}\rho_j(t+2\tau) = {} & 2\rho_j(t+\tau) - \rho_j(t) + a\tau^2\gamma s \\ & \times [\rho_{j+1}(t) - 2\rho_j(t) + \rho_{j-1}(t)] \\ & - a\tau[\rho_j(t+\tau) - \rho_j(t)] \\ & - \tau^2\lambda\gamma s[\rho_{j+2}(t) - 3\rho_{j+1}(t) \\ & + 3\rho_j(t) - \rho_{j-1}(t)] + \tau\lambda[\rho_{j+1}(t+\tau) \\ & - \rho_{j+1}(t) - \rho_j(t+\tau) + \rho_j(t)] \\ & + \tau\gamma s[\rho_{j+1}(t+\tau) - \rho_{j+1}(t) - 2\rho_j(t+\tau) \\ & + 2\rho_j + \rho_{j-1}(t+\tau) - \rho_{j-1}(t)] \\ & - a\tau^2\rho_0^2[V(\rho_{j+1}(t)) - V(\rho_j(t))], \end{aligned} \tag{30}$$

where $s = \rho_0^2 V'(\rho_0)$. The initial conditions of the numerical simulation are set as follows: the lattice number $N = 100$, and the boundary condition is periodical. The density is assumed to be a step function at the average density.

$$\rho_j(0) = \rho_0 = 0.25, \quad j \in [1, N], \tag{31}$$

$$\rho_j(1) = \begin{cases} \rho_0 : & 1 \le j < n_1,\ n_2 < j \le N, \\ \rho_0 + \Delta\rho : & j = n_1, \\ \rho_0 - \Delta\rho : & j = n_2, \end{cases} \tag{32}$$

where $n_1 = 49$, $n_2 = 50$, and $\Delta\rho$ is the initial disturbance.

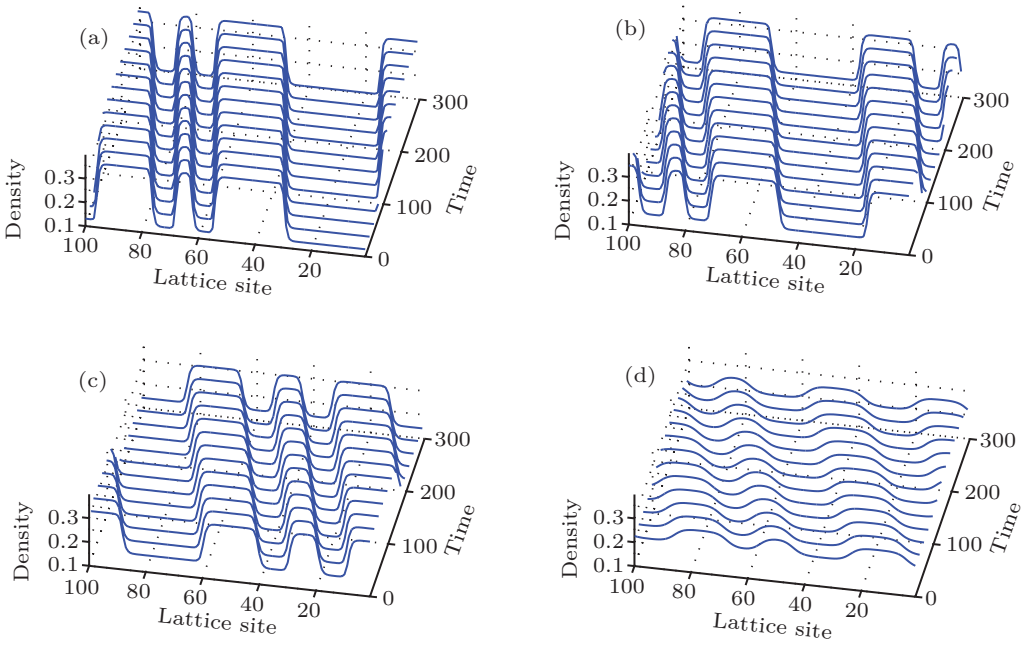


Fig. 3. (colour online) Spatiotemporal evolution of density wave for (a) $\lambda = 0$, (b) 0.1, (c) 0.2, and (d) 0.5 at $t = 10^4$ s with $\gamma = 0.0$ and $\Delta\rho = 0.05$.

Firstly, a numerical simulation for verifying the theoretical result (i.e., the improvement in traffic stability) is performed. Here, we set $a = 0.95$, $\rho_0 = 0.25$, $\rho_c = 0.25$, $\Delta\rho = 0.05$, and $\lambda = 0.0,\ 0.1,\ 0.2$, and 0.5, respectively. Figure 3 shows the spatiotemporal evolution of density waves after a sufficiently long time $t = 10^4$ s with $\gamma = 0.0$. The traffic flow appears unstable since the parameters in Fig. 3 do not satisfy the stability condition (17). Thus, the disturbance will evolve into congested flow, but the scale of density waves is weakened as λ increases. In Fig. 5 where the parameters are the same as those in Fig. 3 except $\gamma = 0.1$, the initial disturbance is amplified in patterns (a), (b), and (c), but is absorbed quickly. The traffic flow is uniform across the whole space in pattern (d). These simulation results demonstrate that both the FDE and the lane changing can stabilize the traffic flow. In addition, the backward kink–antikink density waves can be observed clearly with the evolution of time. The amplitude of density waves decreases with increasing λ. It should be noted that the smaller the amplitude is, the more stable the traffic flow becomes. Therefore, based on the analytical and simulation results, we can conclude that the traffic jam can be suppressed effectively by taking FDE into account. Figures 4 and 6 show the density profiles obtained at $t = 10^4$ s, which correspond to Figs. 3 and 5, respectively.

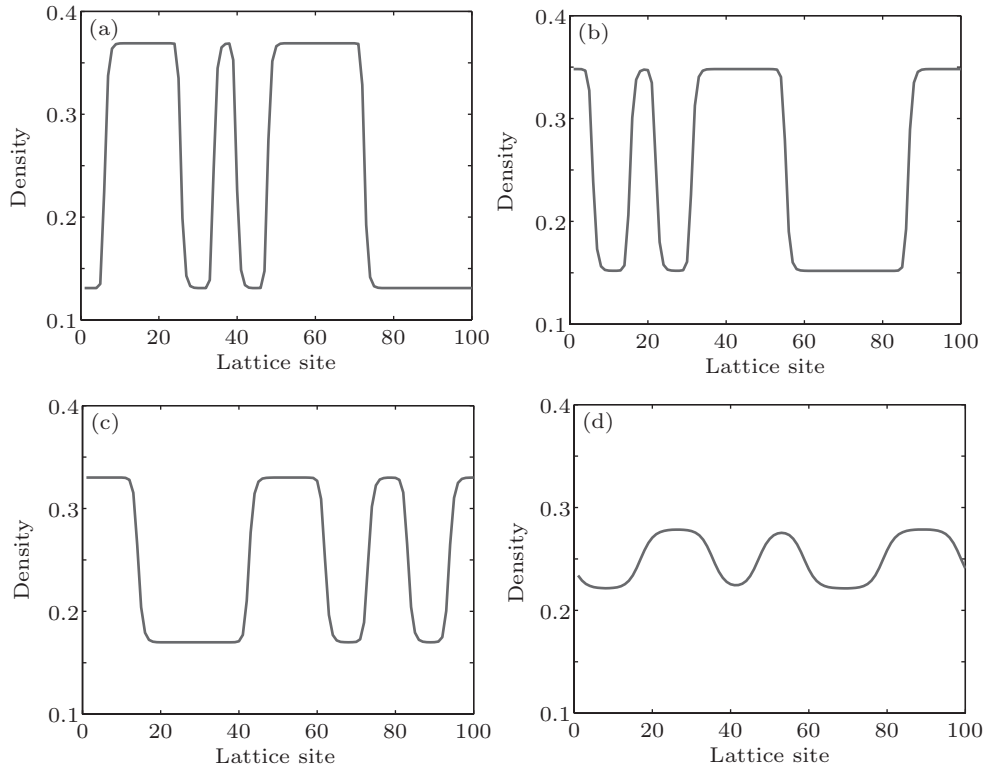


Fig. 4. Density profile for (a) $\lambda = 0.2$ and (b) 0.5 with $\gamma = 0.0$ and $\Delta\rho = 0.05$ at $t = 10^4$ s.

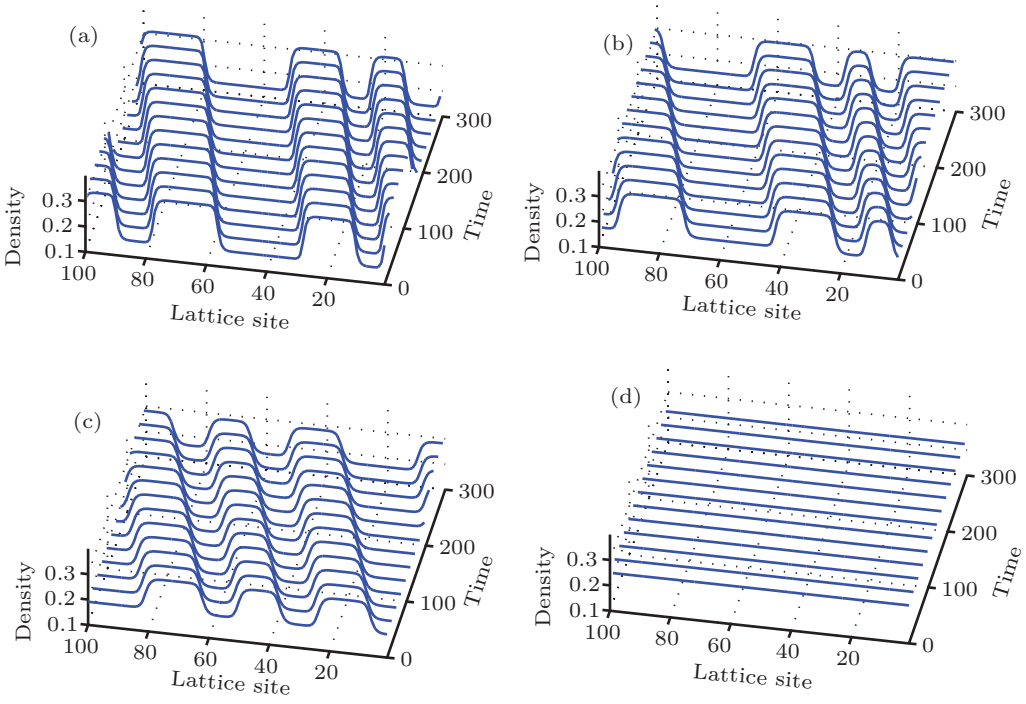


Fig. 5. (colour online) Spatiotemporal evolution of density wave for (a) $\lambda = 0$, (b) 0.1, (c) 0.2, and (d) 0.5 with $\gamma = 0.1$ and $\Delta\rho = 0.05$ at $t = 10^4$ s.

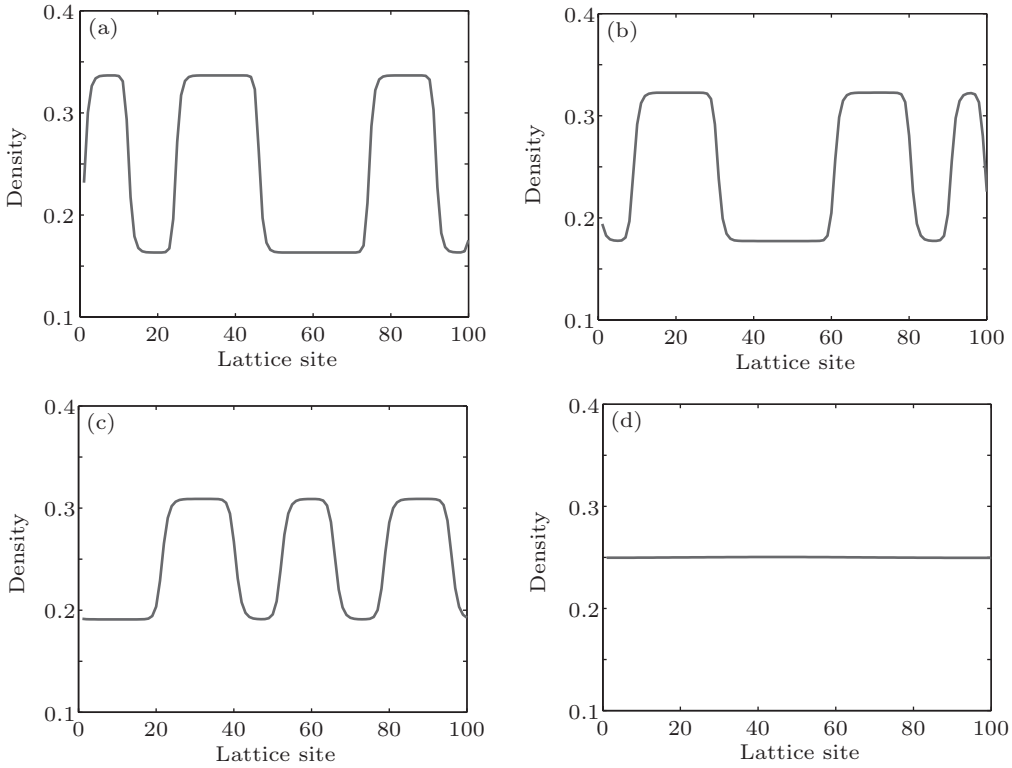


Fig. 6. Density profile for (a) $\lambda = 0$, (b) 0.1, (c) 0.2, and (d) 0.5 with $\gamma = 0.1$ and $\Delta\rho = 0.05$ at $t = 10^4$ s.

Secondly, we investigate whether density waves appear in a metastable region or not when different disturbances are added to the traffic flow. We select two points in a metastable region: one lies in low-density region with $\rho_0 = 0.2$ and $a = 0.9$; the other lies in high-density region with $\rho_0 = 0.3$ and $a = 0.9$.

As is shown in Fig. 7, in a low-density metastable region, when a disturbance is lower than the critical value, the small disturbance ($\Delta\rho < 0.3$) will be absorbed and the traffic flow is uniform. When disturbance is equal to or larger than the critical value ($\Delta\rho = 0.3$), the soliton density waves appear suddenly and propagate backward. The shape and amplitude of soliton density waves will not change with the growing size of disturbance. Figure 8 shows the density profile at $t = 10^4$ s, which corresponds to that in Fig. 7.

In the high-density metastable region (shown in Fig. 9), when the disturbance ($\Delta\rho$) is lower than 0.12, the disturbance dissolves and the traffic flow is stable in whole space. As is shown in Fig. 7, when the disturbance reaches a critical value ($\Delta\rho = 0.13$), kink density waves arise and the traffic flow becomes unstable. In addition, the kink density waves propagate backward and its shape will not change with the disturbance. Figure 10 is the profile of Fig. 9.

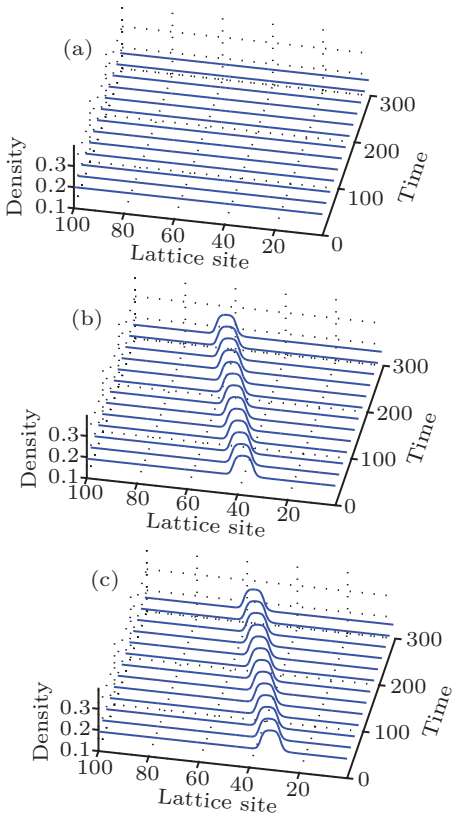


Fig. 7. (colour online) Spatiotemporal evolution of density wave for (a) $\Delta\rho = 0.02$, (b) 0.03, and (c) 0.1 in a low-density metastable region with $\rho_0 = 0.2$ at $t = 10^4$ s.

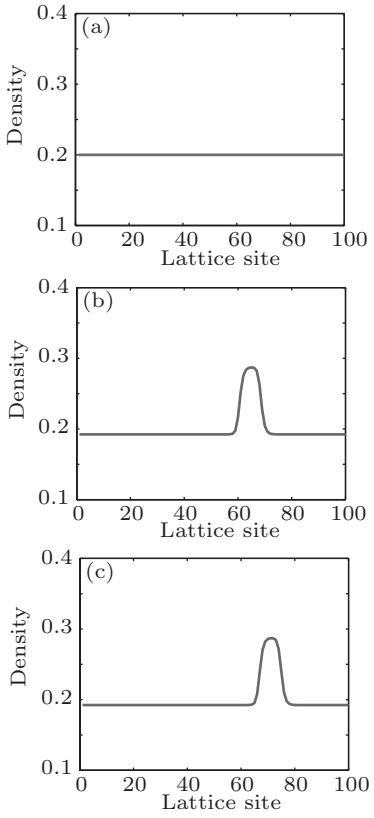


Fig. 8. Density profile for (a) $\Delta\rho = 0.02$, (b) 0.03, and (c) 0.1 in a low-density metastable region with $\rho_0 = 0.2$ at $t = 10^4$ s.

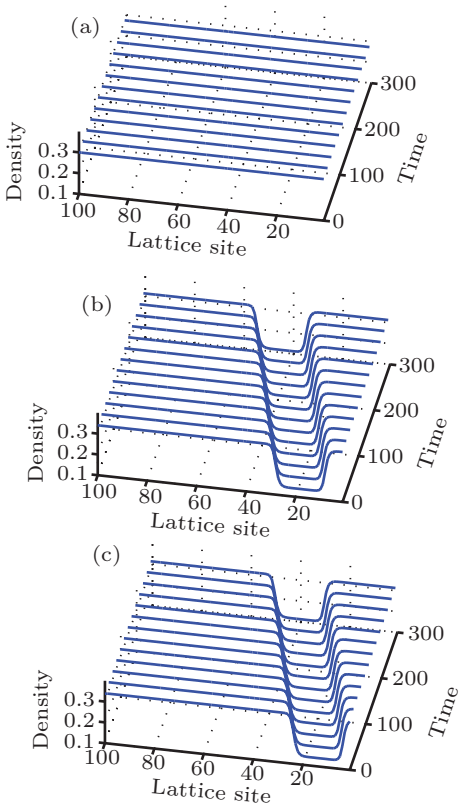


Fig. 9. (colour online) Spatiotemporal evolution of density wave for (a) $\Delta\rho = 0.12$, (b) 0.13, and (c) 0.2 in a high-density metastable region with $\rho_0 = 0.3$ at $t = 10^4$ s.

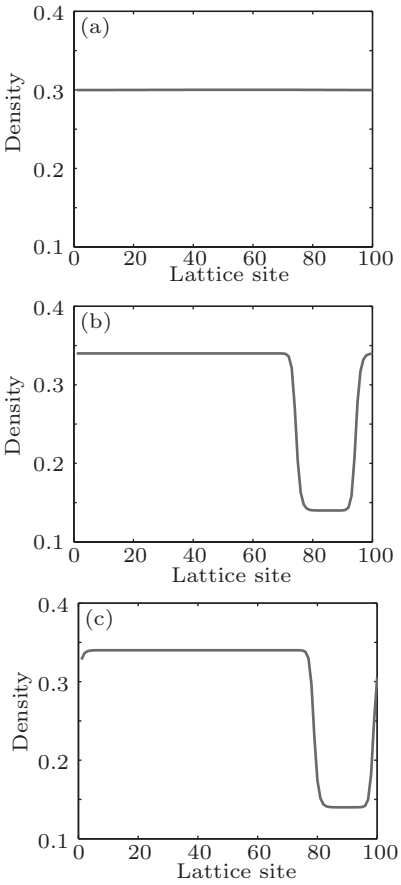


Fig. 10. Density profile for (a) $\Delta\rho = 0.12$, (b) 0.13, and (c) 0.2 in a high-density metastable region with $\rho_0 = 0.3$ at $t = 10^4$ s.

The simulation of different disturbances in a metastable region conforms with the general theory of metastable systems, i.e., a small disturbance decays over time. When a disturbance surpasses a critical value, the disturbance will evolve into unstable traffic state.

6. Conclusion

In this paper, a new two-lane lattice traffic model taking the FDE into account is proposed. With linear and nonlinear analysis methods, the traffic behaviors are investigated analytically. Theoretical results show that the FDE can improve the stability of traffic flow, which are also reproduced by the numerical simulation.

Furthermore, investigation of the evolution laws under different disturbances in the metastable region shows that the soliton density wave occurs at low density, while the kink density wave arises at high density. It coincides with the evolution law of metastable traffic flow.

References

[1] Nagel K and Schreckenberg M 1992 *J. Phys.* **2** 2221

[2] Helbing D 2001 *Rev. Mod. Phys.* **73** 1067

[3] Nagatani T 2002 *Rep. Prog. Phys.* **65** 1331

[4] Zhao X M, Gao Z Y and Jia B 2007 *Physica* A **385** 645

[5] Bando M, Hasebe K, Nakayama A, Shibata A and Sugiyama Y 1995 *Phys. Rev.* E **51** 1035

[6] Jiang R, Hu M B, Jia B, Wang R L and Wu Q S 2007 *Phys. Lett.* A **365** 6

[7] Tian J F, Jia B, Li X G, Jiang R, Zhao X M and Gao Z Y 2009 *Physica* A **388** 4827

[8] Tang T Q, Huang H J and Shang H Y 2010 *Phys. Lett.* A **374** 1668

[9] Nagai R, Nagatani T and Taniguchi N 2005 *Physica* A **350** 548

[10] Kurtze D A and Hong D C 1995 *Phys. Rev.* E **52** 218

[11] Komatsu T and Sasa S 1995 *Phys. Rev.* E **52** 5574

[12] Nagatani T and Nakanishi K 1998 *Phys. Rev.* E **57** 6415

[13] Nagatani T 1998 *Physica* A **261** 599

[14] Nagatani T 1999 *Physica* A **264** 581

[15] Xue Y 2004 *Acta Phys. Sin.* **53** 25 (in Chinese)

[16] GE H X, Dai S Q, Xue Y and Dong L Y 2005 *Phys. Rev.* E **71** 066119

[17] Ge H X and Cheng R J 2008 *Physica* A **387** 6952

[18] Ge H X 2009 *Physica* A **388** 1682

[19] Tian J F, Jia B, Li X G and Gao Z Y 2010 *Chin. Phys.* B **19** 040303

[20] Ge H X, Cheng R J and Lei L 2010 *Physica* A **389** 2825

[21] Tian H H, He H D, Wei Y F, Xue Y and Wei Y F 2009 *Physica* A **388** 2895

[22] Xue Y, Tian H H, He H D, Lu W Z and Wei Y F 2009 *Eur. Phys. J.* B **69** 289

[23] Farah H and Toledo T 2010 *Trans. Res.* F **13** 355

[24] Nagatani T 1999 *Physica* A **265** 297

[25] Tang T Q, Huang H J and Gao Z Y 2005 *Phys. Rev.* E **72** 066124

[26] Huang H J, Tang T Q and Gao Z Y 2006 *Acta Mechanic. Sin.* **22** 131 (in Chinese)

[27] Ge H X, Cheng R J and Dai S Q 2005 *Physica* A **357** 466